

Supplement: A global perspective on the spatial representation of climate extremes from km-scale models

Lukas Brunner¹ (lukas.brunner@uni-hamburg.de), Benjamin Poschlod¹, Emanuel Dutra^{2,3}, Erich M. Fischer⁴, Olivia Martius⁵, and Jana Sillmann¹

¹ Research Unit Sustainability and Climate Risk, Center for Earth System Research and Sustainability (CEN), University of Hamburg, Hamburg, Germany

² Instituto Português do Mar e da Atmosfera, 1749-049 Lisbon, Portugal

³ Instituto Dom Luiz, Faculdade de Ciências, Universidade de Lisboa, 1749-016 Lisbon, Portugal

⁴ Institute for Atmospheric and Climate Science, ETH Zurich, Zurich, Switzerland

⁵ Oeschger Centre for Climate Change Research and Institute of Geography, University of Bern, Bern, Switzerland

Additional supplementary material (database of figures for all ETCCDI indices) can be found online: <https://doi.org/10.5281/zenodo.15613611>

S1 Detailed methods: sub-grid anomaly

In the calculation of the sub-grid anomaly of extreme indices two orders of calculation can be distinguished, that we refer to as “regrid-index” and “index-regrid”.

regrid-index

This approach is taken in the main manuscript as it best highlights the effect of output resolution. It first regrids the base-variables (daily maximum temperature or daily pre-

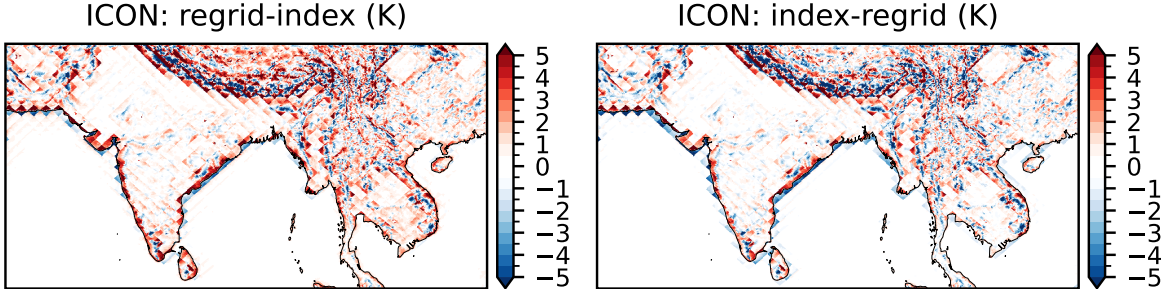


Figure S1: Direct comparison of regridding methods: (left) regrid-index (same as in the main manuscript) and (right) index-regrid for the case of the annual maximum of daily maximum temperature.

cipitation) from zoom level 9 to zoom level 6. A given extreme index is then calculated on both zoom level 9 and 6. Finally, the resolutions are compared.

index-regrid

In the alternative approach a given extreme indices is calculated only once on zoom level 9. The index is then regridded to zoom level 6 and resolutions are compared (figure S1).

For this approach, the mean of all anomalies within one coarse grid cell is zero by definition (which is not the case for the “regrid-index” approach). For the example of the annual maximum of daily maximum temperatures, the differences between resolutions (sub-grid anomalies) are lower for “index-regrid” because the coarse mean is higher: calculating the maximum from a single mean value on zoom level 6 (“regrid-index”) yields a smaller values than calculating the maxima from 64 values on zoom level 9 and then averaging them (“index-regrid”).

S2 Sub-grid anomalies for precipitation

In the main manuscript we describe the sub-grid anomaly for the hottest day in the year (figure 5) with a focus on the Indian sub-continent. Here, we also discuss the corresponding precipitation-based extreme index: the annual maximum of daily precipitation (figures S10 (top row) and S2). Compared to the temperature case, where clear geographical features emerge, precipitation is dominated by the effect of coarsening relatively independent of location. As we use the “regrid-index” approach (see section S1) for all sub-grid

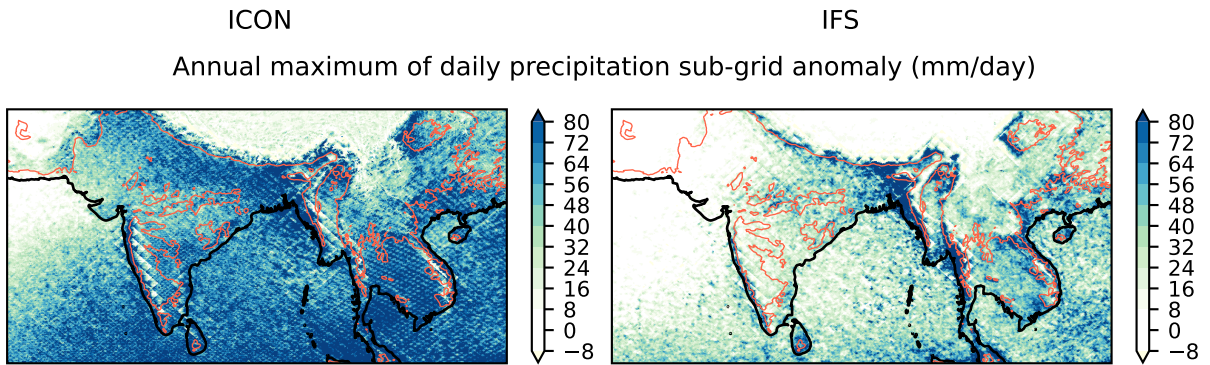


Figure S2: Same as figure 5b in the main manuscript but for the annual maximum of daily precipitation. The red contour-lines indicate 500 m elevation.

anomaly calculations, maximum precipitation is higher everywhere in the zoom level 9 resolution compared to the coarser zoom level 6 resolution. For zoom level 9 the annual maximum is calculated at high resolution capturing small-scale – high-intensity precipitation events. For zoom level 6, in contrast, the daily data are first coarsened averaging out these small-scale events and only then is the annual maximum calculated.

However, topographical features still do play a role, in particular orography as shown in figure S2. For both ICON and IFS the Western Ghats, a mountain range close to the west coast of India, leads to a clearly increased precipitation at zoom level 9. A similar effect can be observed in the north of the Indian sub-continent at the Himalayan mountain range.

S3 City coordinates

The coordinates of the four cities used in the paper are taken from Wikipedia: Karachi (<https://en.wikipedia.org/wiki/Karachi>), Mumbai (<https://en.wikipedia.org/wiki/Mumbai>), Chennai (<https://en.wikipedia.org/wiki/Chennai>), and Kathmandu (<https://en.wikipedia.org/wiki/Kathmandu>). For both the zoom level 9 and zoom level 6 girds the cell with center closest to the city coordinates are taken. The resulting values are summarized in table S1

Table S1: City coordinates (reference) and their interpolated coordinates for the zoom level 9 and zoom level 6 grids.

City	Reference (lat/lon)	Zoom 9 (lat/lon)	Zoom 6 (lat/lon)
Mumbai	19.08°N/72.88°E	19.08°N/72.95°E	18.84°N/73.12°E
Chennai	13.08°N/80.28°E	13.09°N/80.24°E	12.64°N/80.16°E
Karachi	24.86°N/67.01°E	24.87°N/66.97°E	24.62°N/66.80°E
Kathmandu	27.71°N/85.32°E	27.70°N/85.25°E	27.28°N/85.08°E

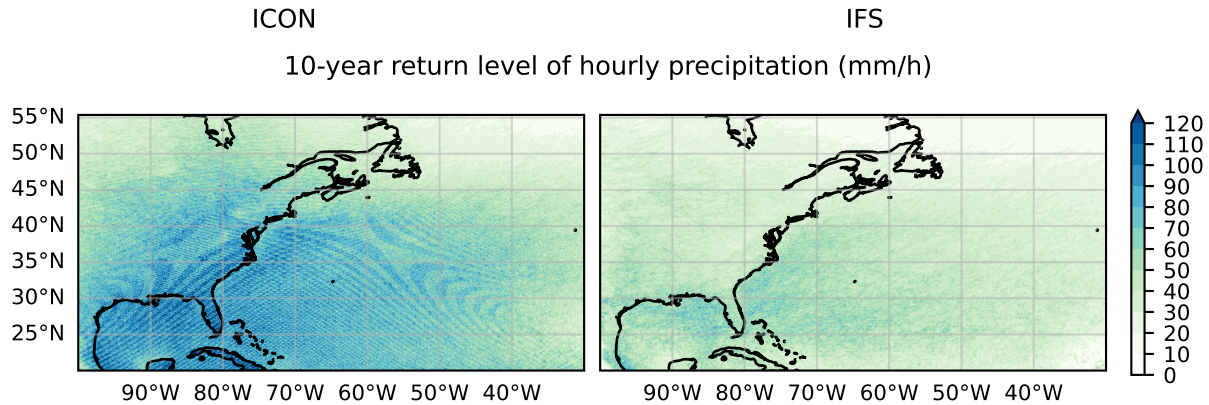


Figure S3: (left) Same as figure 4a in the main manuscript but zoomed into a region with strong Moiré effect in ICON (100°W to 30°W and 20°N to 50°N). (right) The effect is not visible for IFS as it is regredded from a different grid.

S4 Moiré effect in ICON output

We briefly discuss the wave-like patterns visible in the return levels of the ICON model in figure 1 in the main manuscript (e.g., along most of the western edge of the Atlantic and in most Equatorial regions (see figure 4 in the main manuscript and figure S4 for a zoom in). The patterns have so far only emerged for the climatology of hourly return levels and are not visible in more moderate precipitation extremes (figure S6). Additional analysis revealed that these patterns are introduced by interference due to the Moiré effect in the nearest neighbour remapping from the native icosahedral ICON grid to the HEALPix output grid. Since this remapping is done by the ICON model itself the original data is not stored and no re-processing of the data is possible. Overall, the effect is small and does not affect any of our conclusions.

S5 Comparison of absolute and relative indices

The ETCCDI indices features 2 types of extreme thresholds: absolute and relative thresholds. Since they typically capture fundamentally different aspects of extremes, their properties can often not directly be compared. For the example of precipitation, two absolute threshold metrics exist: the number of days exceeding 10mm precipitation per day ($r_{10\text{mm}}$) and the number of days exceeding 20mm ($r_{20\text{mm}}$). In addition, two relative thresholds exist: the sum of precipitation from days where precipitation exceeds the local 95th ($r_{95\text{p}}$) and 99th percentile ($r_{99\text{p}}$). As these two index categories capture conceptually different properties (number of days versus precipitation sums) a direct comparison is not meaningful. A similar consideration holds for temperature extreme indices with the warm and cold spell duration indices capturing a duration (relative threshold), while absolute indices, such as summer or frost days capture a sum of days (absolute threshold).

Yet a comparison of sub-grid properties of absolute and relative threshold-based indices is interesting to isolate differences in their behavior. Here, we use the example of summer days (annual count of days where maximum temperature exceeds 25°) and hot days (annual frequency of days where maximum temperature exceeds its local and seasonally varying 90th percentile). As such they are closely related as, e.g., a hot day frequency of 10 % is equivalent to approximately 36 hot days per year. While we limit our discussion to these two examples here, the conclusions can be generalized also to other indices.

Figure S5 shows different metrics for both indices based on the IFS model. The 29-year mean climatology of summer days reveals a strong latitude dependence, with no summer days occurring at high latitude, a transition region at mid-latitudes, and summer days occurring around the year at low latitudes. In stark contrast, hot days occur exactly 10 % of the time in the 29-year mean by definition, as the same 29 years where used to calculate the 90th percentile (figure S5 top tow).

The sub-grid variability of summer days is discussed in section 3.2 the main manuscript. Here, we show the coefficient of variation in addition. This view is clearly dominated by transition regions (both due to latitude and elevation) where summer days can occur but they are not frequent. The hot day frequency behaves very differently compared to summer days: the amplitude of the sub-grid anomaly is more homogeneous with a maximum at about 5 % (or about 18 days compared to 150 days for summer days). Since the climatology is also very homogeneous, the pattern hardly changes between the standard deviation and the coefficient of variation in contrast to the summer days. The effect of coastlines and topography is also greatly reduced. Yet, some imprint of topography and land-sea contrasts remains even for hot days as also discussed in the main manuscript.

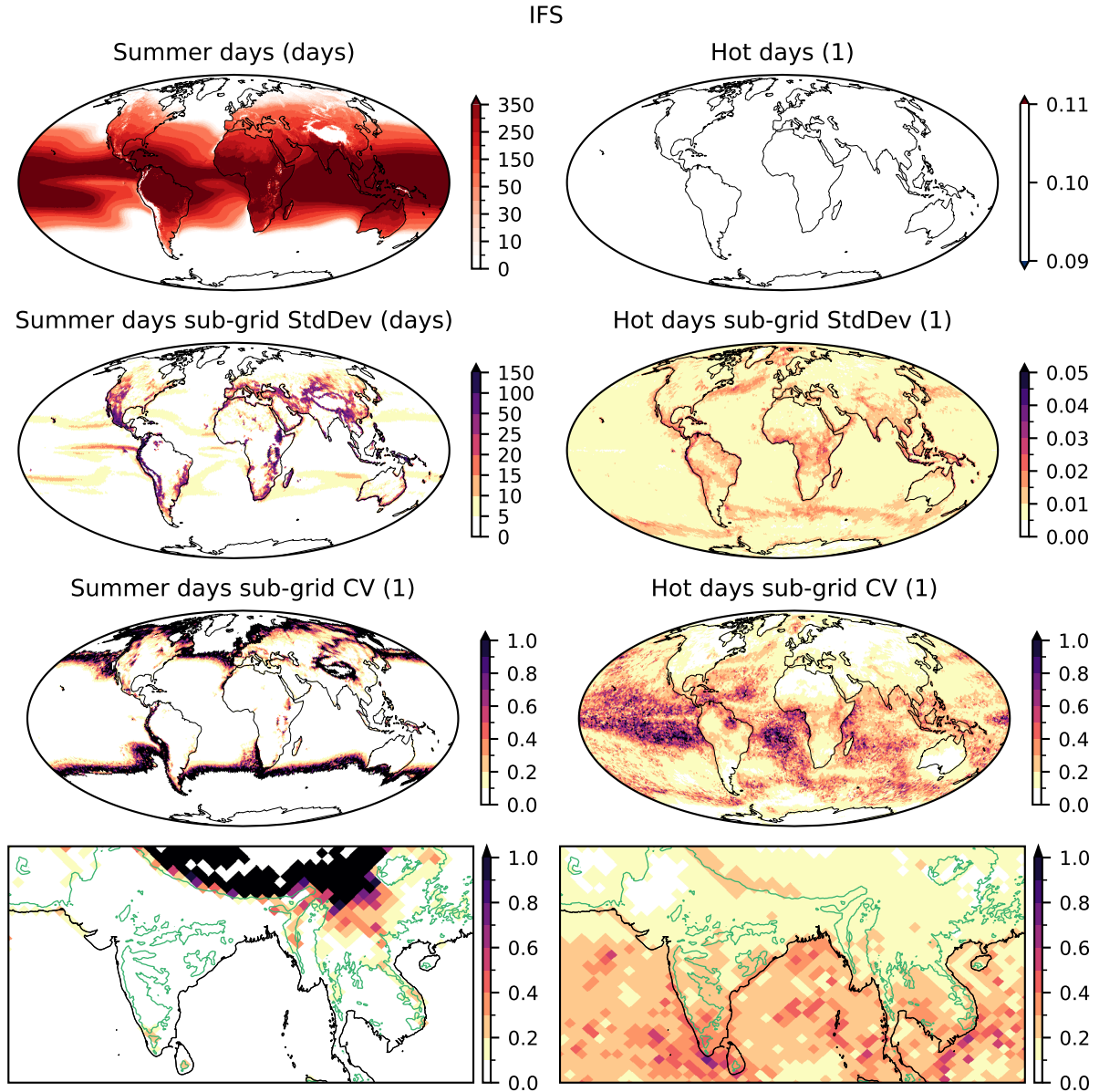


Figure S4: Comparison of an absolute (summer days) and relative (hot days) threshold-based extreme index. (top) 29-year mean climatology, (2nd row) sub-grid anomaly, and (bottom rows) coefficient of variation (standard deviation divided by mean). Note that for hot days the 29-year mean value is 10% everywhere by definition, corresponding to about 36 hot days per year. The range of the coefficient of variation is fixed to the same range to ease comparability.

S6 Additional figures

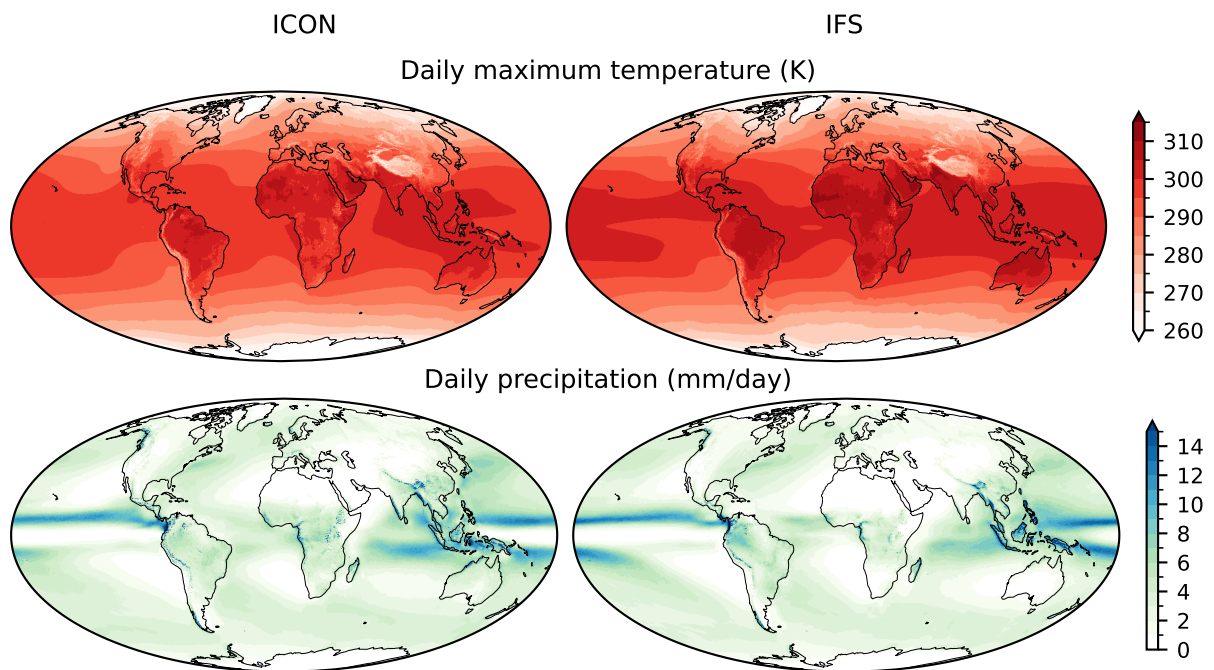


Figure S5: 2021-2049 mean for (top) daily maximum temperature and (bottom) daily precipitation from (left) ICON and (right) IFS.

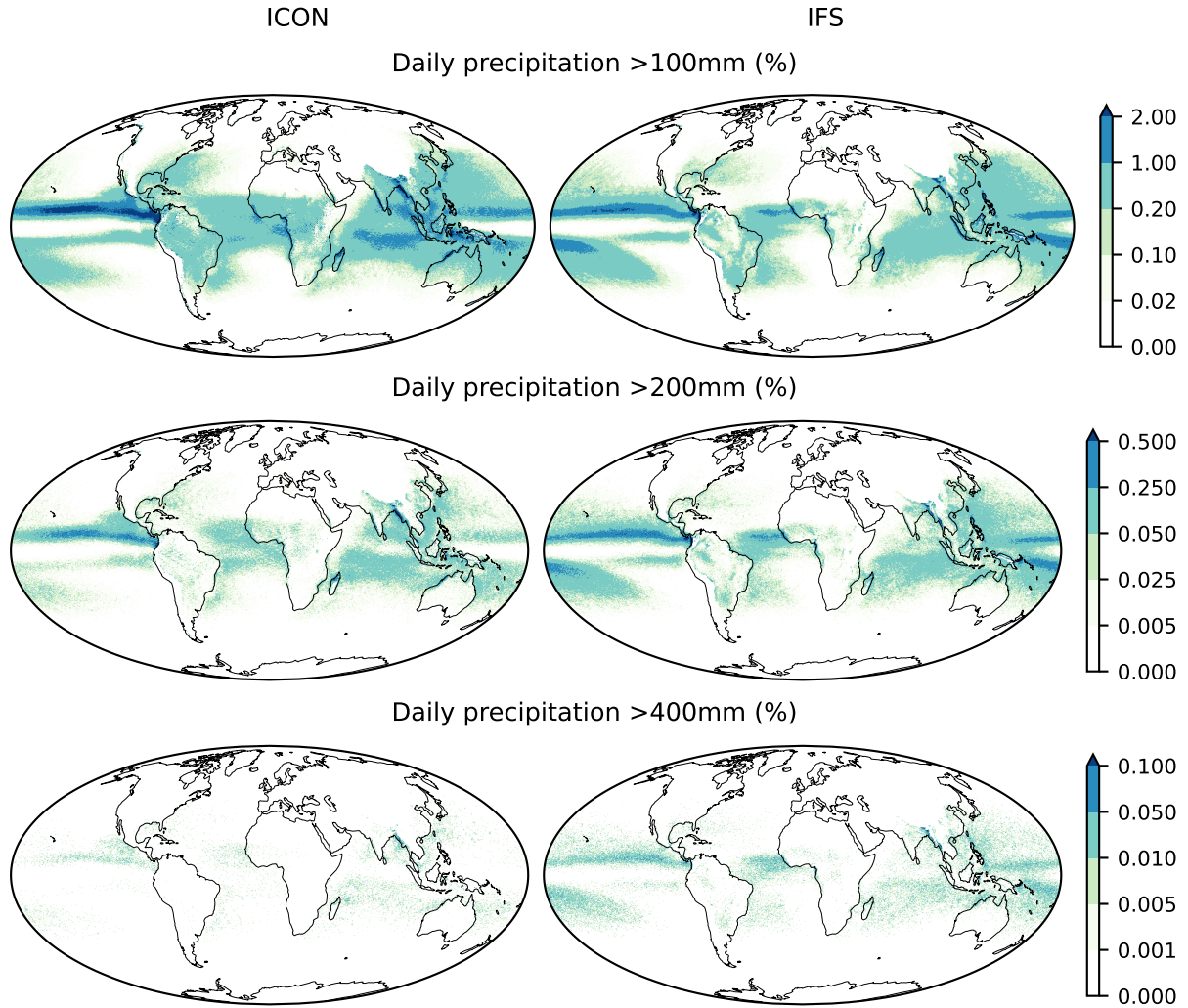


Figure S6: Frequency of daily precipitation exceeding 400 mm for (left) ICON and (right) IFS.

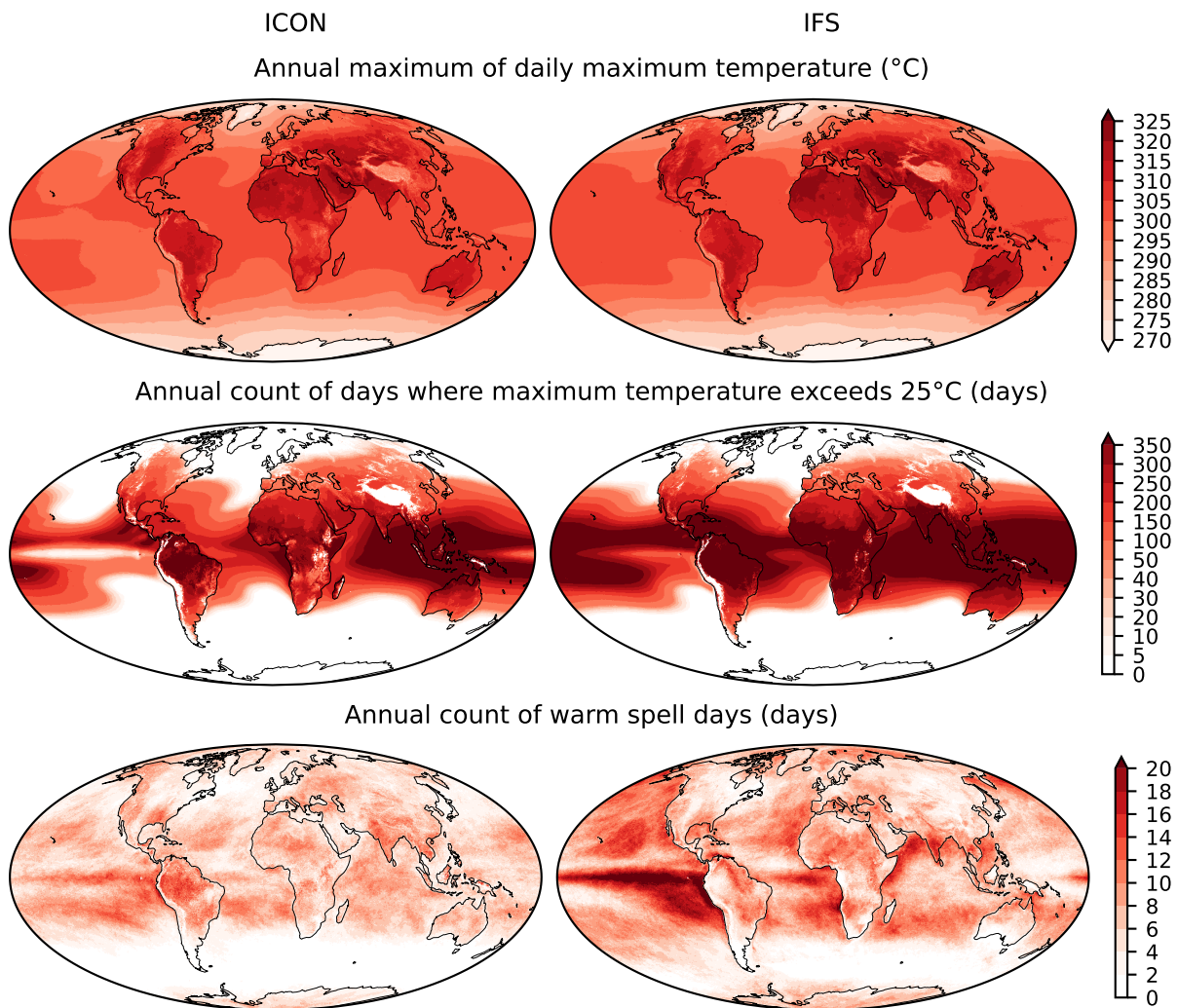


Figure S7: 2021-2049 mean for the three heat metrics used in figure 2 in the main manuscript: (top) annual maximum of daily maximum temperature, (middle) summer days (maximum temperature $> 25^{\circ}\text{C}$), and (bottom) warm spell duration index (sum of days where maximum temperature is above the 90th percentile for at least six consecutive days) for (left) ICON and (right) IFS.

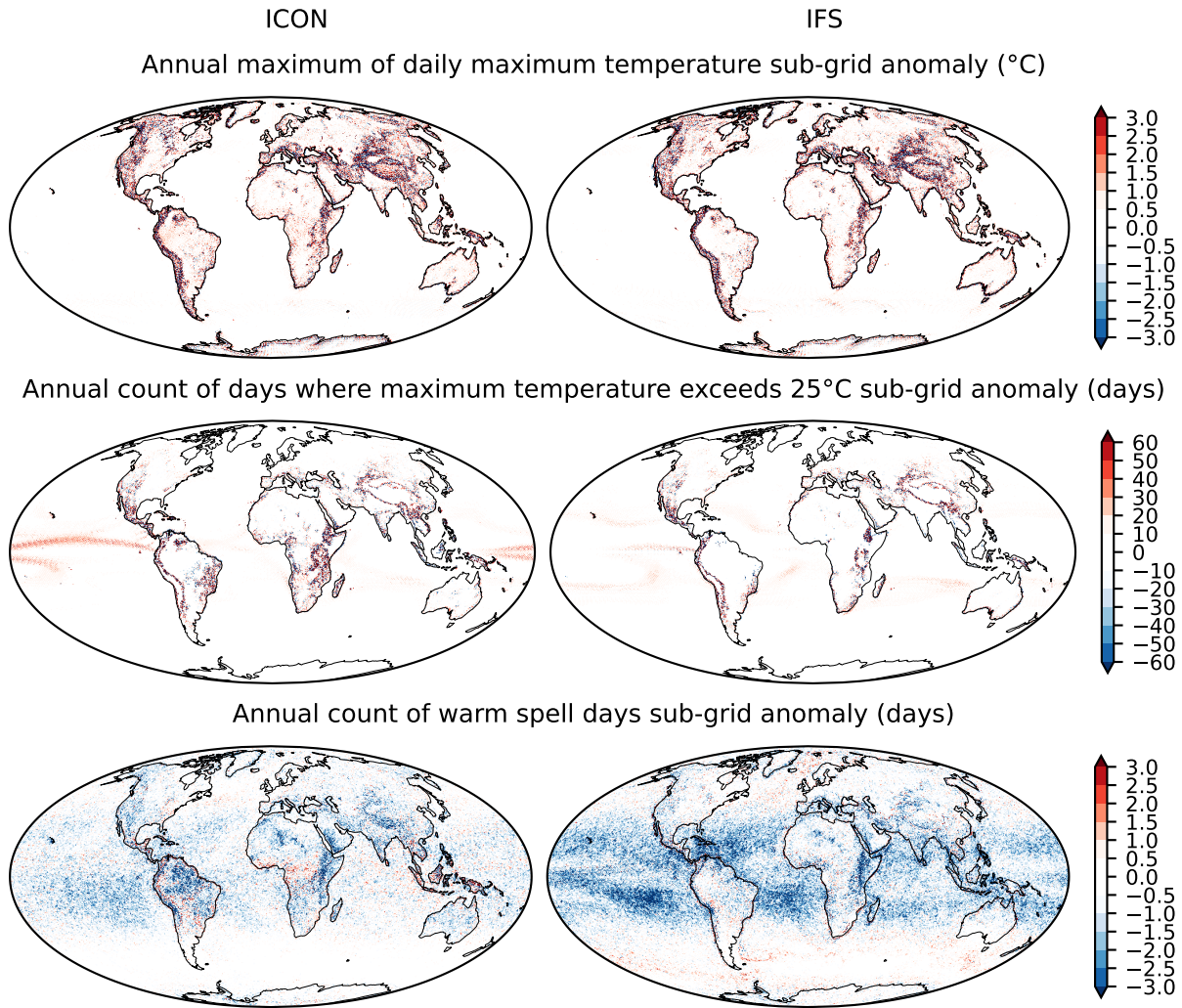


Figure S8: Sub-grid anomaly for the three heat metrics shown in figure 2 in the main manuscript: (top) annual maximum of daily maximum temperature, (middle) summer days (maximum temperature $> 25^{\circ}\text{C}$), and (bottom) warm spell duration index (sum of days where maximum temperature is above the 90th percentile for at least six consecutive days) for (left) ICON and (right) IFS.

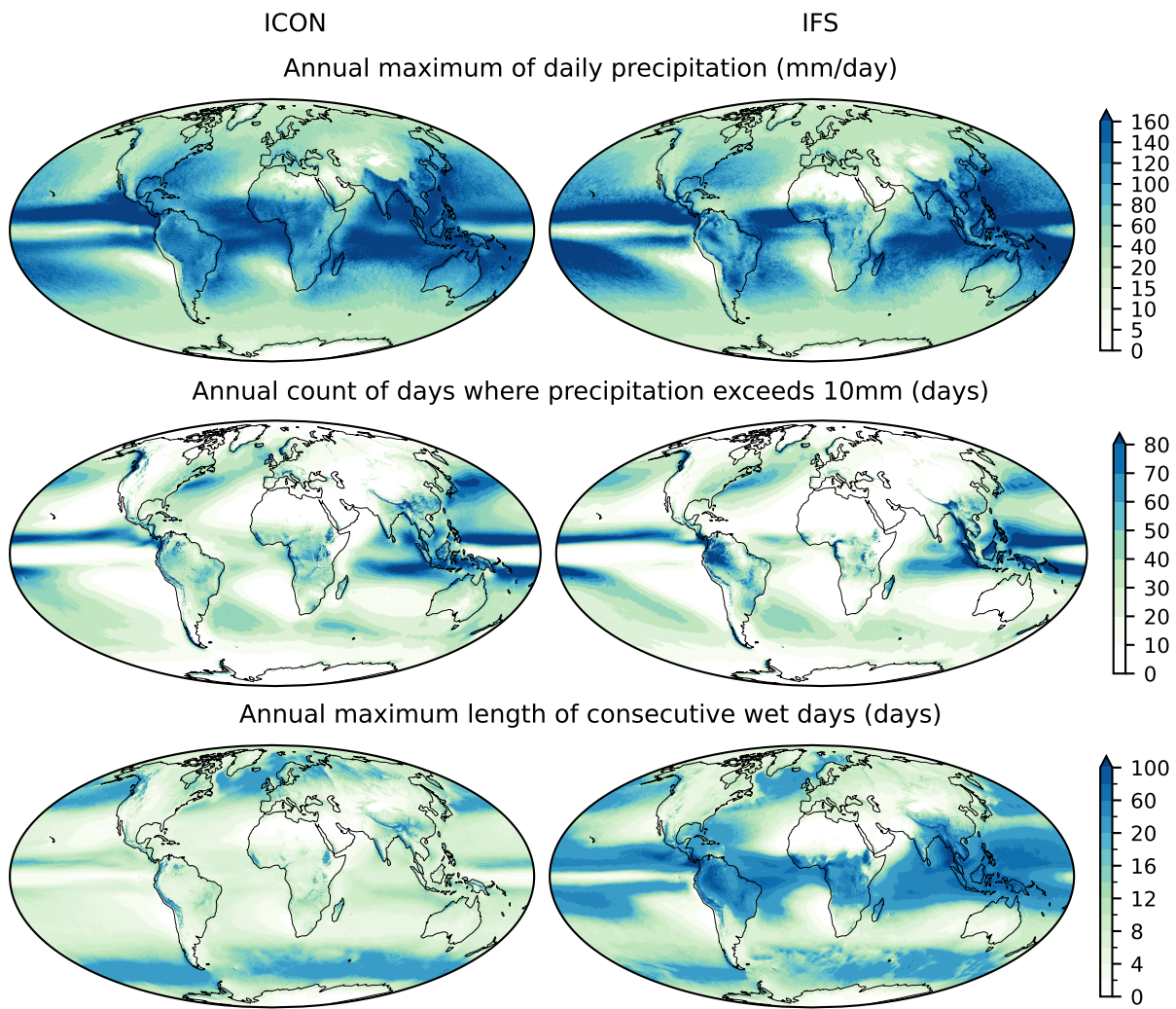


Figure S9: 2021-2049 mean for the three precipitation metrics shown in figure 3 in the main manuscript: (top) annual maximum of daily precipitation, (middle) number of heavy rain days (daily precipitation > 10 mm), and (bottom) maximum annual length of consecutive wet days (daily precipitation > 1 mm) for (left) ICON and (right) IFS.

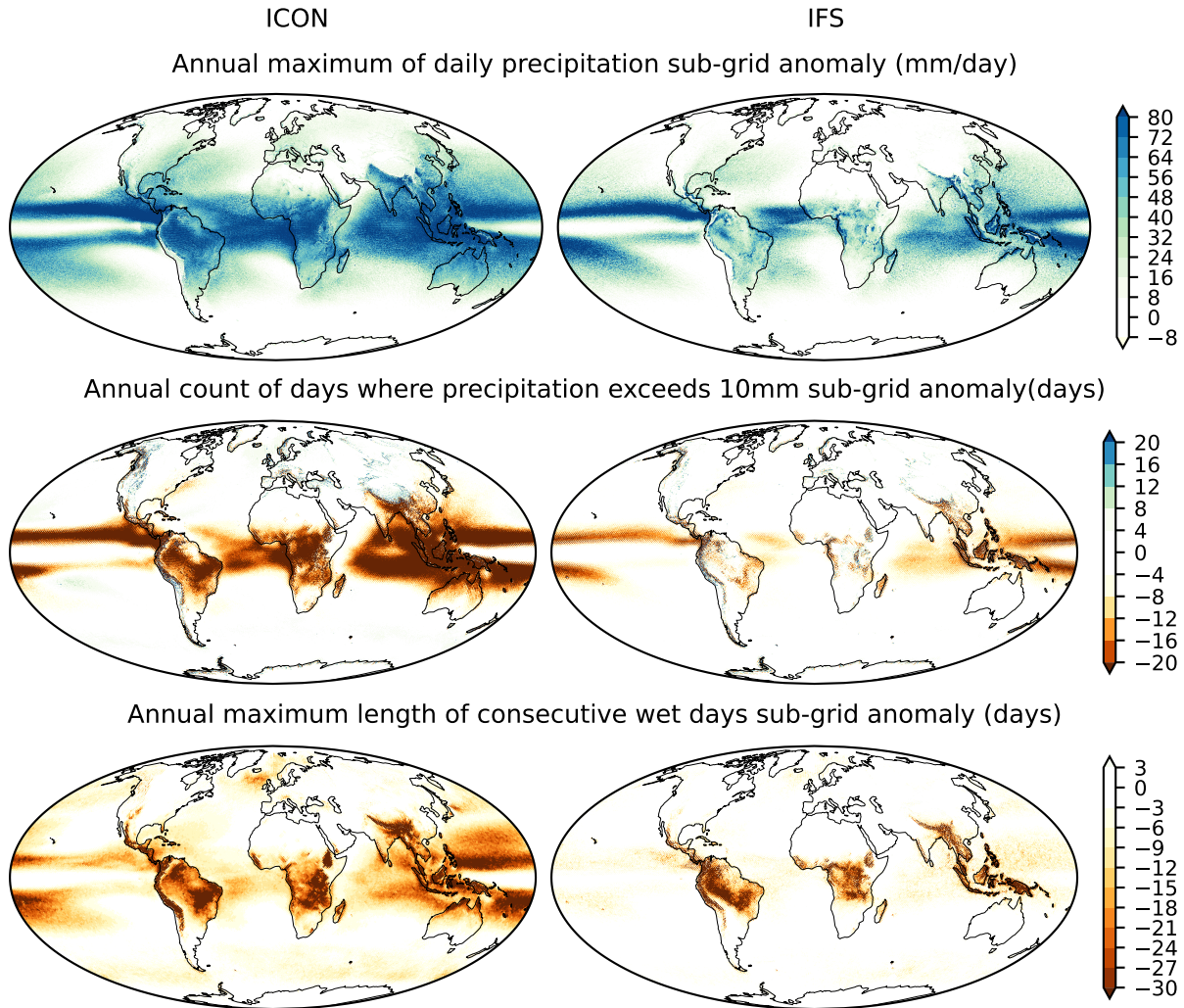


Figure S10: Sub-grid anomaly mean for the three precipitation metrics shown in figure 3 in the main manuscript: (top) annual maximum of daily precipitation, (middle) number of heavy rain days (daily precipitation $> 10 \text{ mm}$), and (bottom) maximum annual length of consecutive wet days (daily precipitation $> 1 \text{ mm}$) for (left) ICON and (right) IFS.

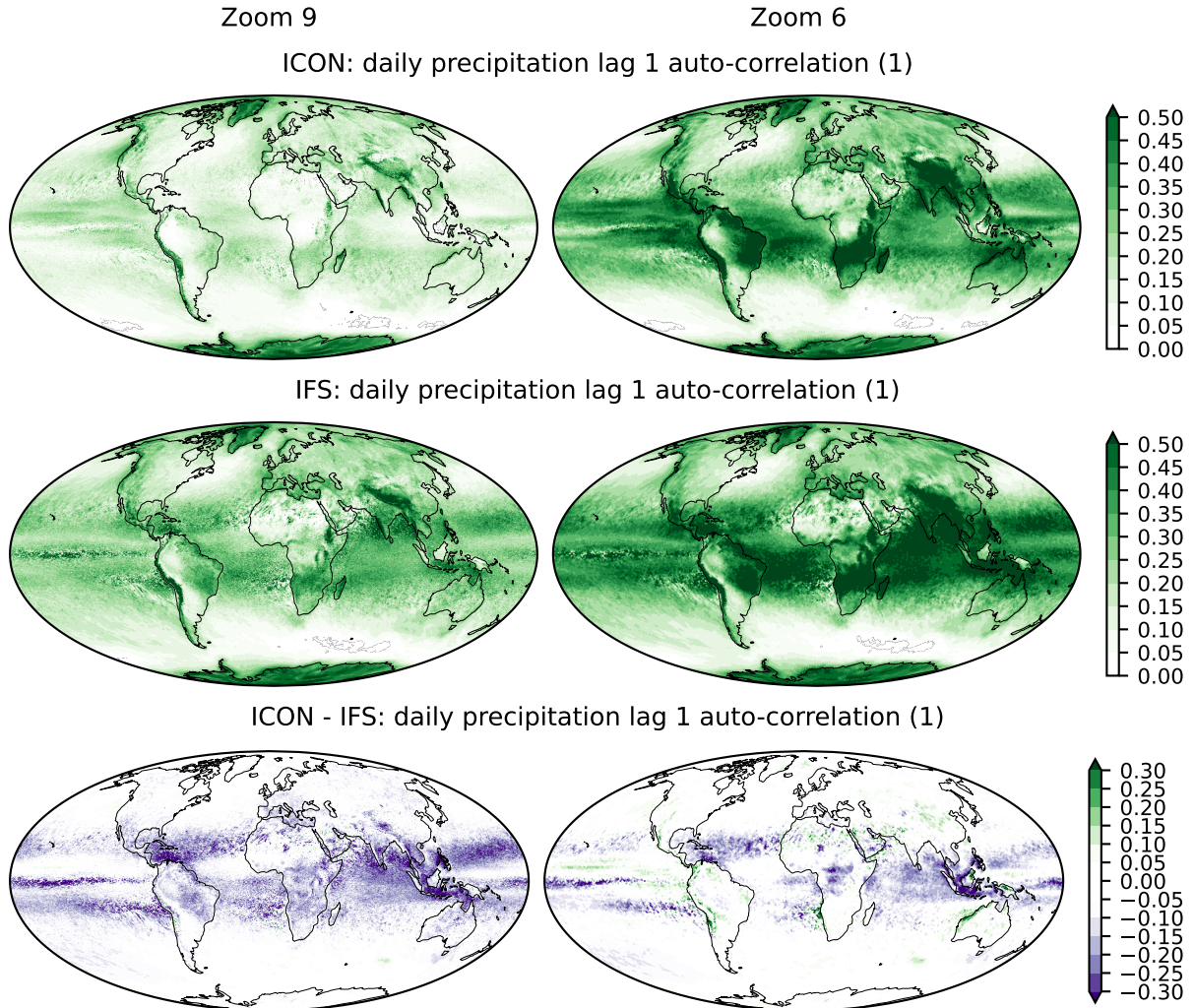


Figure S11: Daily precipitation lag 1 auto-correlation in the period 2021-2049 for (top) ICON, (middle) IFS, and (bottom) their difference. The left column shows zoom level 9, the right one zoom level 6.

Annual maximum length of consecutive wet days sub-grid cv (1)

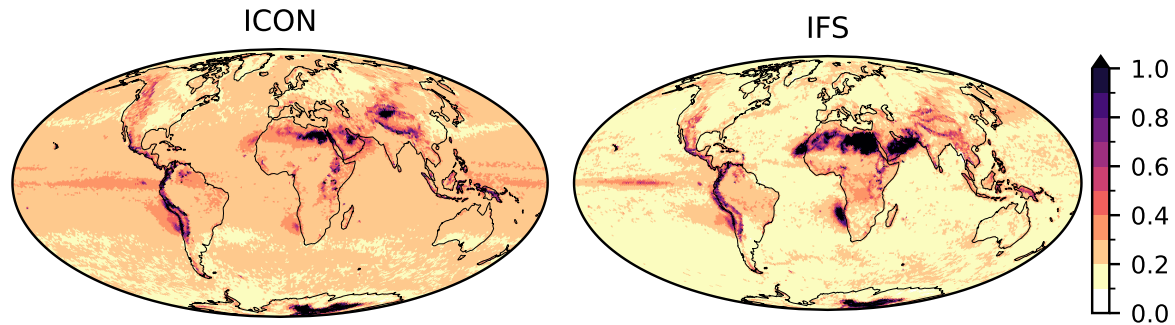


Figure S12: Sub-grid coefficient of variation for maximum annual length of consecutive wet days (daily precipitation > 1 mm) for (left) ICON and (right) IFS.

ICON: Ocean fraction sub-grid standard deviation (1)

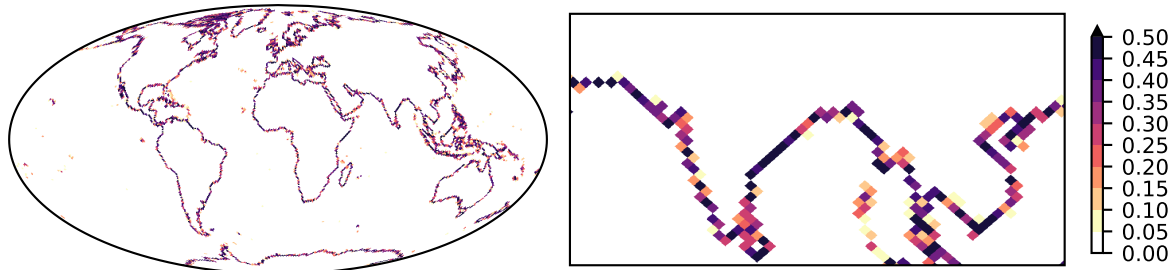


Figure S13: ICON ocean fraction sub-grid variability (left) and zoom-in on the Indian sub-continent (right).

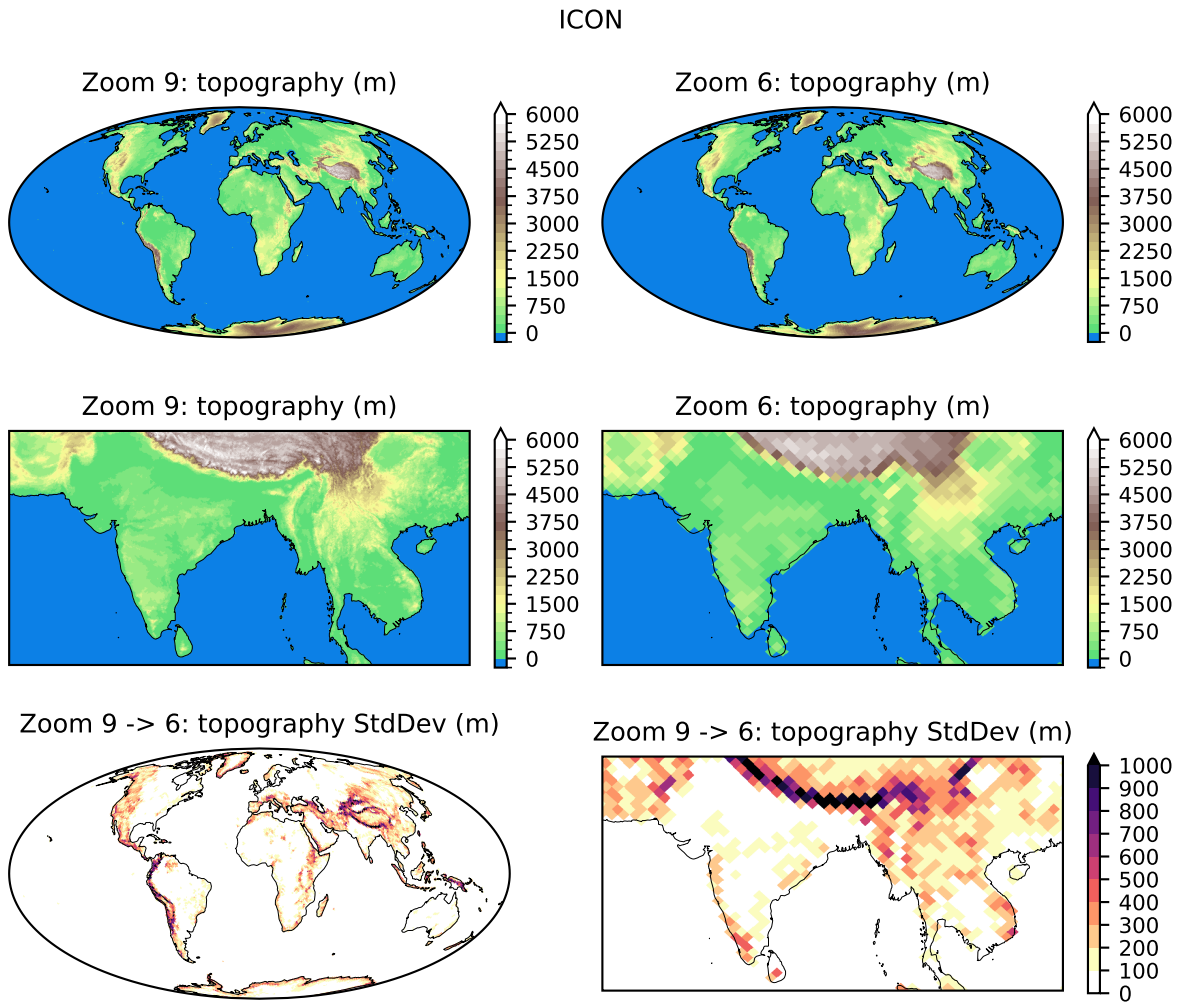


Figure S14: (top) ICON land topography at (left) zoom level 9 and (right) zoom level 6. (bottom left) Sub-grid variability of the topography and (bottom right) sub-grid anomaly of topography in the Indian region. Cells with more than 50 % ocean fraction at a given resolution are shown in blue in the upper panels.